ELSEVIER

Journal of South American Earth Sciences 23 (2007) 242–255

Journal of
South American
Earth Sciences

www.elsevier.com/locate/jsames

The Cipoeiro gold deposit, Gurupi Belt, Brazil: Geology, chlorite geochemistry, and stable isotope study

Evandro L. Klein [a,*], Chris Harris [b,1], André Giret [b], Candido A.V. Moura [c]

[a] CPRM/Geological Survey of Brazil. Av. Dr. Freitas, 3645, Belém-PA CEP: 66095-110, Brazil
[b] Université Jean Monnet, Département de Géologie. 23, rue du Docteur Paul Michelon, 42000, Saint Etienne, Cedex 2, France
[c] Laboratório de Geologia Isotópica – Para-Iso, Universidade Federal do Pará, Centro de Geociências, CP 1611, Belém-PA CEP: 66075-900, Brazil

Received 1 August 2004; accepted 1 May 2006

Abstract

The Cipoeiro gold deposit, located in the Gurupi Belt, northern Brazil, is hosted by tonalites of 2148 Ma. The deposit is controlled by splays related to the major strike-slip Tentugal shear zone, and at the deposit scale, the mineralization is confined to ductile–brittle shear zones. Mineralization style comprises thick quartz veins and narrow and discontinuous quartz-carbonate veinlets associated with disseminations in altered host rocks. The postmetamorphic hydrothermal paragenesis is composed of quartz, calcite, chlorite, white mica (phengite), pyrite, and minor albite. Electron microprobe analysis of chlorites reveals a relatively uniform chemical composition at depths of more than 100 m. The chlorites are characterized by (Fe + Mg) ratios between 0.37 and 0.47 and Al^{IV} ranging between 2.22 and 2.59 a.p.f.u. and are classified as Fe-chlinochlore. Temperatures calculated by applying the Al^{IV} contents of chlorites yield a relatively narrow interval of 305 ± 15°C. Stable isotope (O, H, C, S) compositions have been determined in silicate, carbonate, and sulfide minerals. The $\delta^{18}O$ and δD values of the mineralizing fluid range from +2.4 to +5.7 and from −43‰ to −20‰, respectively, and are interpreted as having a metamorphic origin. The $\delta^{13}C$ values of fluid CO_2 are in the range −10.7‰ to −3.9‰, whereas the fluid $\delta^{34}S$ is around 0‰. Carbon and sulfur compositions are not diagnostic of their sources, compatible as they are with mantle, magmatic, or average crustal reservoirs. The hydrothermal paragenesis, chlorite–pyrite coexistence, temperature of ore formation, and sulfur isotope evidence indicate relatively reduced fO_2 conditions for the mineralizing fluid. Geologic, chemical, and isotopic characteristics of the Cipoeiro deposit are compatible with the class of orogenic gold deposits.

Keywords: Stable isotope; Gold; Thermometry; Gurupi Belt; Chlorite

1. Introduction

Cipoeiro and the nearby Chega Tudo gold deposits hold the most important known gold concentration of the plutonometamorphic Gurupi Belt in northern Brazil (Fig. 1), with grouped geologic resources of about 60 tonnes Au grading 1.4 g/t (Torresini, 2000). Geologic, geophysical, and structural aspects of these deposits are relatively well constrained (Torresini, 2000; Ribeiro, 2002), but genetic information is not available. It is the intention of this study to discuss some genetic aspects of the Cipoeiro deposit. We provide chemical data for hydrothermal chlorites and stable isotope (O, H, C, S) compositions of silicate, carbonate, and sulfide minerals. These chemical and isotopic results, in addition to field, structural, and petrographic information, enable us to discuss genetic variables of the Cipoeiro deposit, including temperature and redox conditions of ore deposition, as well as possible sources for fluids and metals.

* Corresponding author. Tel.: +55 3276 8577; fax: +55 3276 4020.
E-mail address: eklein@be.cprm.gov.br (E.L. Klein).
[1] Present address: Department of Geological Sciences, University of Cape Town, Rondebosch 7700, South Africa.

0895-9811/$ - see front matter © 2006 Elsevier Ltd. All rights reserved.
doi:10.1016/j.jsames.2006.09.002

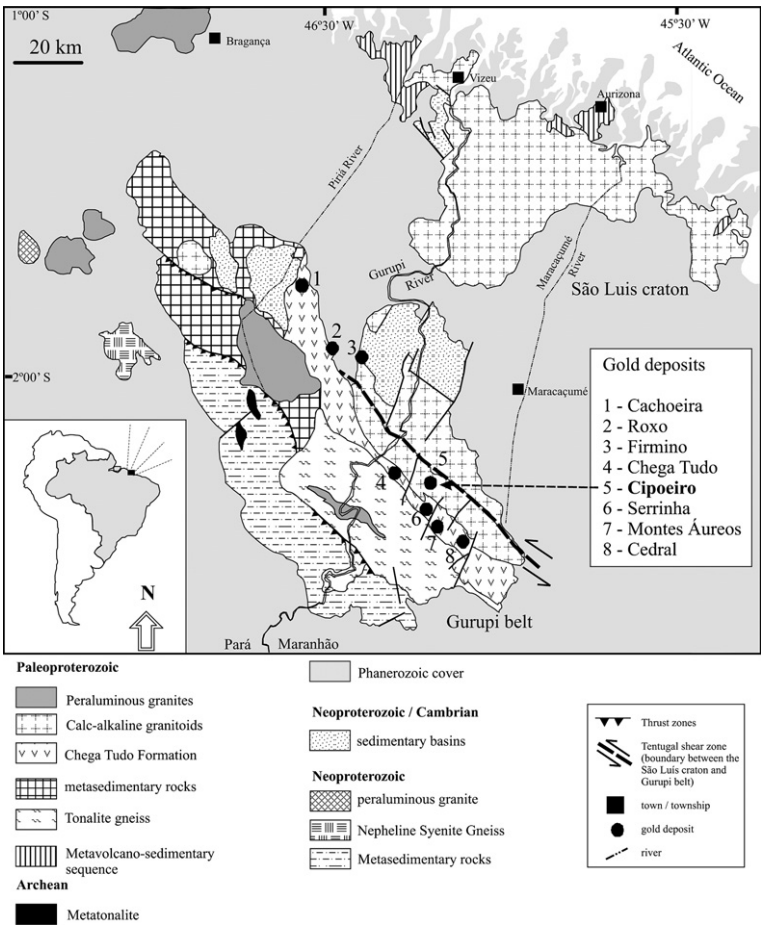

Fig. 1. Simplified geologic map of the São Luis Craton and Gurupi Belt, showing the location of Cipoeiro and other gold deposits.

2. Geologic overview

The Cipoeiro gold deposit is located within the Tentugal shear zone, in the boundary zone between the São Luís Craton and the Gurupi Belt in northern Brazil (Fig. 1). The host shear zone is an approximately 120 km long and 15–30 km wide strike-slip corridor of intense deformation that records sinistral displacements (Costa et al., 1988; Ribeiro, 2002). Most of the known gold deposits in the Gurupi Belt are associated with this structure. The São Luis Craton comprises suites of calc-alkaline granitoids showing single zircon Pb-evaporation ages ranging from 2165 to 2149 Ma (Klein and Moura, 2001, 2003) and younger peraluminous granites of 2090 Ma (Palheta, 2001). These granitoid suites underwent very low-grade metamorphism at a regional scale and intruded older greenschist to lower-amphibolite facies metavolcanosedimentary rocks dated at 2240 Ma (Klein and Moura, 2001). Cratonization is estimated to have occurred at about 1900 Ma, according to Rb–Sr and K–Ar evidence (see the review in Klein and Moura, 2003 for primary references).

The Gurupi Belt consists of NNW–SSE-trending metavolcanosedimentary and sedimentary sequences with intercalated massifs of gneiss and metatonalite, in addition to intrusions of calc-alkaline granitoids, muscovite-bearing leucogranites, and alkaline rocks (Fig. 1). The volcanosedimentary and sedimentary successions are composed of detrital sedimentary rocks with intercalations of felsic, intermediate, and subordinate mafic volcanic rocks and metachert. These sequences underwent metamorphism under variable conditions, from subgreenschist to amphibolite facies (Pastana, 1995; Costa et al., 1996; Yamaguti and Villas, 2003), and the rocks show a pervasive NW–SE-striking schistosity and/or mylonitic fabric that dip at moderate to high angles generally to the SW. The volcanosedimentary sequence shows Pb-evaporation zircon ages in the range of 2148–2160 Ma (Klein and Moura, 2001), whereas the metasedimentary successions are positioned in both the Paleoproterozoic and Neoproterozoic (Klein et al., 2005). Medium- to higher-amphibolite facies tonalite gneisses show a crystallization age of 2167 ± 2.5 Ma (Klein et al., 2005). Distinct generations of calc-alkaline and peraluminous granitoids supposedly intruded the supracrustal sequences at 2159 and 2100–2080 Ma, respectively (Palheta, 2001; Klein et al., 2005). The latter are likely related to a collisional event that took place in the region at the end of the orogenic process that spanned approximately 2240–2080 Ma (Palheta, 2001; Klein and Moura, 2003; Klein et al., 2005). The Gurupi Belt also records evidence of Neoproterozoic extensional and orogenic events, defined

by the intrusion of a nepheline-bearing syenite at 730 Ma and a late- to posttectonic muscovite-bearing granite at 550 Ma (Palheta, 2001; Klein et al., 2005). Neoproterozoic ages in the 600–650 Ma range have also been recorded in detrital zircons from sedimentary rocks of a small basin located close to the boundary between the São Luís Craton and the Gurupi Belt (Pinheiro et al., 2003).

3. Geology of the gold deposit

The host rocks for the gold mineralization at Cipoeiro comprise variably altered and sheared tonalites that occur in tectonic contact with a metasedimentary sequence composed of magnetite-rich metasandstone and metapelite (Fig. 2) with lenses of metaconglomerate (Torresini, 2000). The tonalites belong to the major suite of calc-alkaline granitoids of the São Luís Craton that have been affected by the deformation imparted by the Tentugal shear zone. A sample of these tonalites taken from a drill core in the Cipoeiro deposit yield a zircon Pb-evaporation age of 2148 ± 4 Ma (Klein and Moura, 2001).

Integrated structural and lithological mapping and geophysical information allowed Ribeiro (2002) to define a corridor of highly strained rocks striking dominantly N40°W, occurring 8–10 km south of the Cipoeiro deposit. This corridor is a structural domain of the Tentugal shear zone that developed in the contact between metavolcanosedimentary rocks and the tonalites that host the gold mineralization at Cipoeiro, as a consequence of the competency contrast presented by these two adjacent rock units. Accordingly, the fine-grained schists and metavolcanic rocks concentrated strain and displacements, whereas the coarse-grained tonalites are relatively less deformed (Ribeiro, 2002). As part of the structural evolution, Ribeiro

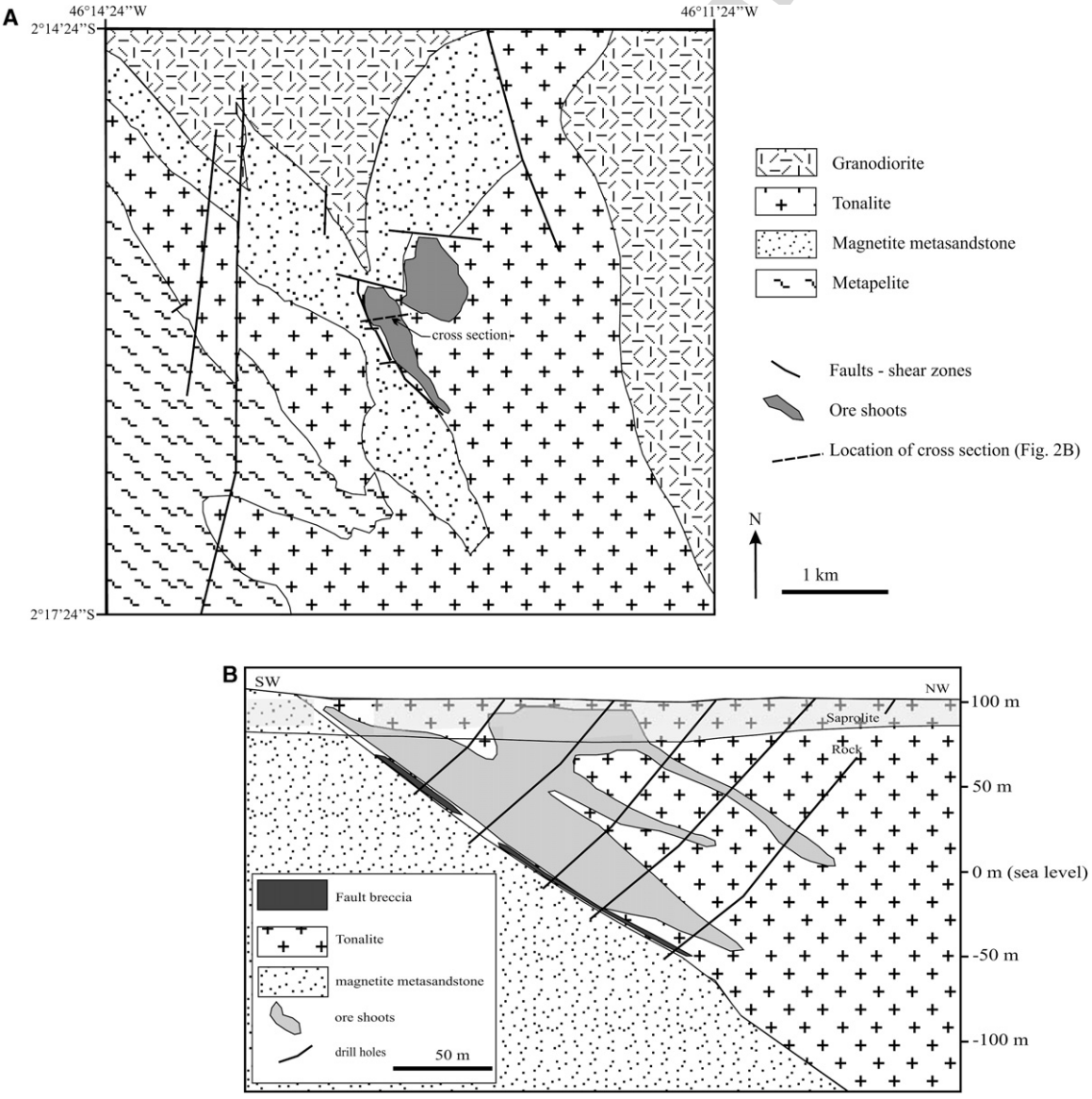

Fig. 2. (A) Geologic map of the Cipoeiro deposit area (after Torresini, 2000). (B) Cross-section of the Cipoeiro deposit (after Torresini, 2000).

(2002) also describes the formation of N–S-trending fault systems and splays that subsequently have been reactivated and displaced by small-scale thrusts and E–W-striking strike-slip faults. The Cipoeiro deposit is located in these geometrically related splays.

At the deposit scale, the deformation at Cipoeiro concentrated in discrete shear zones that cut the hosting tonalites. The least deformed tonalites show preserved igneous textures (Fig. 3A), with plagioclase phenocrysts set in a medium-grained matrix composed of quartz, plagioclase, and hornblende, along with titanite, zircon, and apatite as accessory phases. In more deformed and hydrothermally altered zones, the primary texture and mineralogy have been modified totally, with the original rocks transformed in fine-grained foliated rocks (Fig. 3A).

Drilling in the deposit area down to 250 m revealed several mineralized zones with variable thickness and gold grades ranging from 0.3 to 2 ppm. The ore bodies occur near the faulted contact between the tonalite and the magnetite-rich metasandstone; the contact is outlined by fault breccias (Fig. 2). The fault system is conformable with the regional structural trend (NW–SE) of the Gurupi Belt, dipping 40–70° to the NE, and combines displacements parallel to this regional trend, along with reverse faults. Furthermore, the original structure of the deposit has been modified by late faults that fragmented, displaced, and rotated the ore shoots (Ribeiro, 2002). The ore shoots are entirely hosted by the sheared tonalite and confined to ductile and brittle–ductile shear zones restricted to the hangingwall of the fault (Torresini, 2000; Ribeiro, 2002).

The styles of mineralization comprise basically thick quartz veins and disseminations in discrete shear zones (Fig. 3). The quartz veins show a milky to smoky and massive aspect (Fig. 3A) and are a few tens of cm thick. They have variable angle relationships with the foliated host rocks, both concordant and discordant with respect to the foliation, and gold was deposited at the vein–wall rock contact. The vein quartz underwent recrystallization, which eliminated and/or modified nearly all fluid inclusions. The remaining inclusions are too small for conventional microthermometry and petrography. Furthermore, this recrystallized character indicates that the thick quartz veins were deposited early in the hydrothermal evolution of the deposit.

In the disseminated style, the host shear zones are up to a few meters wide; within these zones, the rocks are variably foliated (Fig. 3A), and the foliation is kinked and moderately folded. In addition, the rocks are pervasively and strongly altered. The hydrothermal alteration that accompanied gold mineralization produced an assemblage consisting of quartz, chlorite, white mica, calcite, albite, and pyrite. This alteration assemblage overprinted the greenschist facies metamorphic assemblage of the host tonalite and is compatible with greenschist facies conditions. The alteration is compositionally homogeneous over 100 m in depth, varying in the amount of each mineral phase. Quartz occurs in small composite (quartz–

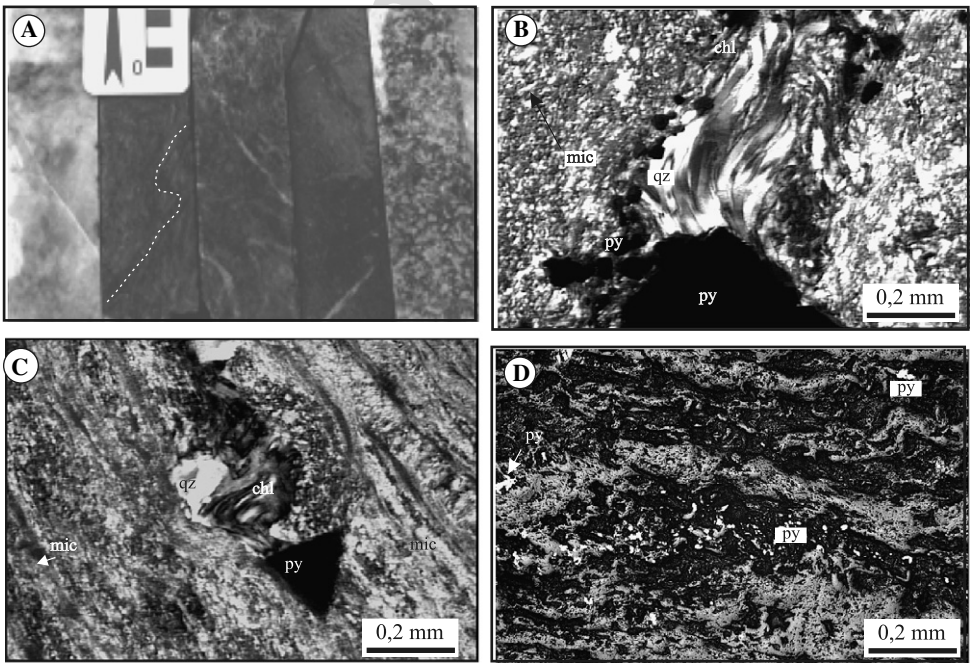

Fig. 3. (A) Photograph of drill core slabs showing aspects of the host rocks and mineralization styles at Cipoeiro. Least-altered tonalite (right) shows preserved igneous texture. Variably altered and deformed tonalite (three slabs in the middle) with primary texture totally destroyed; note the weakly folded foliation (outlined by the white dashed line) and the narrow quartz-carbonate veinlets (white). Thick milky massive quartz vein (left). (B–C) Photomicrographs showing textures and mineralogy of the alteration assemblage. (B) Coarse- to fine-grained pyrite (py) with quartz (qz) in strain fringes and white mica (mic) in the fine-grained matrix. (C) Coarse- to fine-grained pyrite (py) with aggregates of chlorite (chl) and quartz (qz) in strain fringes and white mica (mic) defining the foliation. (D) Stringers of pyrite (py) in the foliation planes formed by gangue minerals (gray and black groundmass).

carbonate) veinlets (Fig. 3A), in aggregates of recrystallized grains in strain fringes of pyrite crystals, whether associated or not with chlorite (Fig. 3B and C). Chlorite is generally the most abundant phase and shows ubiquitous association with pyrite, occurring normally in strain fringes of this sulfide. In places, it forms fibrous aggregates. White mica is more important in the level 201 m, where it is stretched and distributed as stringers along the foliation planes and mainly defines the mylonitic foliation (Fig. 3C). Albite is a very subordinate phase, mostly restricted to the intermediate portion of the deposit. Pyrite shows variable shapes (anhedral to euhedral), sizes, and distribution. In general, it forms medium- to coarse-grained grains (Fig. 3B and C), but in more deformed and folded portions of the host rocks, it tends to form stringers of fine-grained anhedral crystals (Fig. 3D). This tendency likely represents dissolution and reprecipitation of pyrite in response to deformation. Calcite is widespread, occurring in veinlets with quartz (Fig. 3A), and disseminated in the fine-grained hydrothermal matrix, forming up to 10% of the mineral assemblage. Gold is rarely visible and mostly detected chemically. The higher grades are intimately associated with pyrite concentrations and quartz–carbonate–sulfide veinlets precipitated in small-scale brittle–ductile shears, fractures, and veins (Ribeiro, 2002). This observation defines the late-tectonic character of gold precipitation.

Textural and cross-cutting relationships between phases of the alteration assemblage of the pervasive stage are not always clear, and deformation contributed to the difficulty of establishing the paragenetic sequence. A tentative ordering of the paragenesis is illustrated in Fig. 4. As a whole, quartz, carbonate, chlorite, white mica, and pyrite coexisted in the main alteration stage. In places, chlorite and white mica are juxtaposed, whereas in other places, the white mica appears to have crystallized in fractures or cleavage planes of chlorite crystals. Most of the calcite crystals are subhedral, but in places, some crystals clearly display deformation features, indicating that they started to be precipitated early in the alteration evolution. However, some larger crystals of calcite involve small chlorite and white mica crystals, and calcite fills some microcracks that cut across the pervasive alteration, indicating that carbonate crystallization outlasted late brittle fracturing.

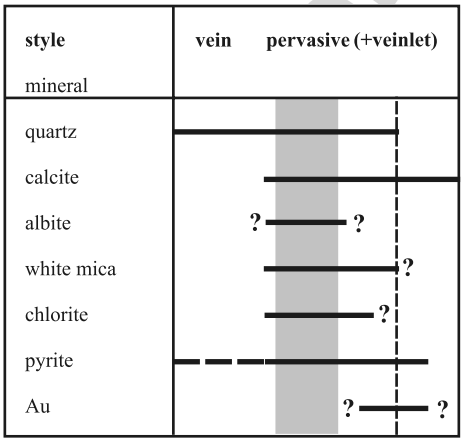

Fig. 4. Schematic paragenetic sequence of alteration minerals in veins and pervasive stages in the Cipoeiro deposit. The shaded area corresponds to the likely relative timing of ductile–brittle deformation, and the vertical dashed line defines the late brittle fracturing.

Absolute timing of the mineralizing episode has not been determined, but it is considered to postdate the metamorphic peak in the Gurupi Belt, which is estimated to have occurred at about 2080–2100 Ma, on the basis of the age of the emplacement of the peraluminous (collision-type) granitoids (Palheta, 2001; Klein and Moura, 2003; Klein et al., 2005).

4. Sampling and analytical procedures

Microprobe analyses of hydrothermal chlorite have been carried out at the Université Blaise Pascal in Clermont Ferrand, France, using a Cameca SX-100 probe, coupled with a BSE system. Acceleration voltage was 15 kV, with 10 seconds counting time per element. Calibration was done with available natural and synthetic standards. FeO was considered as total iron, and H_2O was calculated by stoichiometry. The analytical results have been recalculated on the basis of chlorite formula with 36 oxygen atoms (O, OH), 16 groups of OH, and 8 atoms of $Si + AL^{IV}$ – that is, on the basis of 28 atoms of oxygen per formula unit (a.p.f.u.). White mica analyses have been recalculated to 24 atoms per formula unit (a.p.f.u.), 4 OH groups, and 8 atoms of $Si + AL^{IV}$.

Carbon, oxygen, and hydrogen isotope studies in carbonate and silicate minerals and inclusion fluids were carried out at the Laboratoire des Isotopes Stables of the Université Jean Monnet (UJM) in Saint Etienne, France. Isotope ratios were measured with a Micromass-Isoprime gas-source mass spectrometer using the dual-inlet procedure. Sulfur isotopes were analyzed in a Finnigan MAT 252 mass spectrometer at the Stable Isotope and ICP/MS laboratory of the Queen's University, Kingston, Canada. Carbon dioxide was released from calcite by reaction with 100% H_3PO_4 (McRae, 1950). Analytical precision determined from duplicates is 0.2‰ for both $\delta^{13}C$ and $\delta^{18}O$. For oxygen analysis of silicate minerals, two methods were employed, both using BrF_5 as reagent. The conventional fluorination method (Clayton and Mayeda, 1963) was employed for white mica and chlorite, whereas a CO_2 laser fluorination system (Harris et al., 2000) was used for quartz analysis. In both methods, oxygen was converted to CO_2 by reaction with graphite. An internal standard (MQ quartz, $\delta^{18}O = 10.1‰$) was analyzed to calibrate the data to the SMOW scale, giving an average difference of 0.3‰ between analyses. Hydrogen was produced by heating mineral concentrates in a vacuum, following procedures described by

Vennemann and O'Neil (1993), with water reduced to H_2 by reaction with zinc at 450 °C, according to procedures adapted from Coleman et al. (1982). An internal silicate standard (AM muscovite, $\delta D = -30‰$) furnished an average value of $-30.5‰$, used to calibrate the data for the SMOW scale. Reproducibility is estimated to be better than 4‰. Inclusion fluids were liberated by thermal decrepitation at temperatures >800 °C from inclusions contained in previously cleaned (HCl and HNO_3) and degassed quartz. Water and a CO_2 fraction were recovered and analyzed for hydrogen and carbon isotopes, respectively. For sulfur analysis, SO_2 was produced from 3 to 5 mg of pyrite loaded into tin capsules and reacted with CuO at 1400 °C in a He stream, using the thermal conversion/elemental analyzer–isotope ratio mass spectrometer technique. The analytical uncertainty for $\delta^{34}S$ is 0.5‰. The $^{13}C/^{12}C$, $^{18}O/^{16}O$, D/H, and $^{34}S/^{32}S$ ratios are all reported in delta notation, relative to the PDB (carbon), SMOW (oxygen and hydrogen), and CDT (sulfur) scales.

5. Mineral chemistry and chlorite geothermometry

5.1. Chlorite and white mica chemistry

The chemical composition of chlorites has been determined in samples from depths of 103 m (upper level), 185 m (intermediate level), and 201–216 m (lower level). The upper level corresponds to an altered but weakly mineralized microtonalite, and the intermediate and lower levels are mineralized zones in tonalites. The results (Tables 1–3) show that the chlorites from the different zones have broadly the same composition, with global values of the Fe/(Fe + Mg) ratios ranging from 0.37 to 0.47 and Al^{IV} values varying between 2.22 and 2.59 a.p.f.u. This small variability suggests that chemical equilibrium of chlorites and hydrothermal fluid has been attained. Two compositional types have been defined – ripidolites and picnochlorites (Fig. 5A) – according to Hey's (1954) classification. According to Bayliss's (1975) classification, as recommended by Bailey (1980), the chlorites are of the Fe-clinochlore type.

Limited analyses ($n = 5$) of white mica from the 103 m (upper level, microtonalite-hosted) and 201 m (lower level, tonalite-hosted) levels of the Cipoeiro deposit have been performed to define the type of the mineral. The results are presented in Table 4 and show that the white micas have relatively constant and similar compositions in the two levels, with average Si, Al^{IV}, and K of 6.6, 1.35, and 1.95 a.p.f.u., respectively. Compositionally, the white micas belong to the phengitic series, intermediate members of the muscovite–celadonite solid solution series.

5.2. Chlorite geothermometry

The empirical chlorite thermometry (Kranidiotis and MacLean, 1987; Cathelineau, 1988; Zang and Fyfe, 1995) is based on the variation of Al^{IV} content and Fe/(Fe + Mg) ratios of chlorites as a function of temperature. Some problems in the application of this empirical geothermometer include contamination of chlorites by submicroscopic inclusions or interlayers (Schiffman and Fridleifsson, 1991; Jiang et al., 1994). Contaminated chlorites typically have variable amounts of Ca + Na + K. To avoid this concern, only analyses with Ca + Na + K < 0.5 a.p.f.u. have been used in the temperature calculations, as suggested by Vidal et al. (2001). In addition, the Fe/(Fe + Mg) ratio and formation temperatures may be influenced by the fluid-to-rock ratio, fO_2, fS_2, pH, and the composition of the hydrothermal fluid and host rock (Kranidiotis and MacLean, 1987; De Caritat et al., 1993; Jiang et al., 1994), parameters that are not always readily available.

Despite these limitations, the use of the chlorite chemical composition to estimate the temperature of ore formation is an effective procedure, provided that some basic principles are observed, namely: (1) consistency between the chemical data of the studied chlorites and those of chlorites used in the calibration of the geothermometers; (2) correlation between the Fe/(Fe + Mg) ratio and Al^{IV} contents; and (3) the results are compared with independent temperature estimations.

Because chlorite is a common mineral in the hydrothermal assemblage in the Cipoeiro deposit, the commonly used empirical geothermometers were employed to constrain the temperature of the chlorite (and the hydrothermal system) formation in this deposit, in line with the preceding conditions. The Fe/(Fe + Mg) ratios and Al^{IV} show a positive correlation (Fig. 5B), and the determined chemical values fall within the compositional range of the chlorites used by Kranidiotis and MacLean (1987) to calibrate their geothermometer. Accordingly, temperatures calculated using this geothermometer (Tables 1–3, Fig. 5C) better represent the conditions of precipitation of the hydrothermal chlorites at Cipoeiro. Temperatures calculated using the calibrations of Cathelineau (1988) and Zang and Fyfe (1995) yield systematically higher and lower values (Tables 1–3), respectively. The sample of the 103 m level shows temperatures between 308 and 325 °C, with well-defined modal and average values of 315 °C. The sample of the 185 m level shows more spread values, with an average value of 302 ± 12 °C, but most values are in the 290–305 °C range. The sample of the level 201 m shows a majority of values between 295° and 315 °C, with a mean value of 305 ± 9 °C. Sample 103 (weakly mineralized microtonalite) shows a slightly higher average temperature but not significantly different (<13 °C) from the two other samples (mineralized tonalite). In summary, the total range of temperatures is 282–327 °C, and most values are in the 290–320 °C interval (Fig. 5C). The modal value of 305 °C, taken from the chlorite composition of the altered and mineralized tonalites, is assumed to be the best approximation of the formation temperature of the chlorites.

Table 1
Chemical composition of hydrothermal chlorites of the Cipoeiro deposit (level 103 m)

Analysis	29	30	31	32	34	35	36	38	39	40	41	42	43	45	46	48	50	52	54	55	56	58	59
SiO_2 (wt%)	26.53	26.31	25.92	26.33	26.36	26.10	25.57	26.19	25.86	26.59	25.96	26.39	26.54	26.23	27.07	27.41	26.49	26.15	26.14	26.52	26.44	26.23	26.30
Al_2O_3	20.48	20.28	20.36	19.49	20.09	20.34	19.35	20.10	20.85	20.43	19.70	20.43	20.71	20.24	20.48	19.79	20.78	20.91	20.50	20.78	20.26	18.72	20.55
FeO	23.81	24.01	23.85	23.52	23.38	23.74	23.25	23.57	23.46	24.25	23.17	23.17	23.38	23.84	23.39	23.37	23.68	23.03	23.67	23.53	23.49	23.74	23.64
MnO	0.46	0.45	0.51	0.44	0.51	0.50	0.47	0.46	0.51	0.58	0.52	0.50	0.48	0.51	0.48	0.52	0.49	0.46	0.49	0.49	0.46	0.58	0.54
MgO	16.72	16.82	16.71	17.22	17.07	15.63	16.75	17.33	16.79	16.51	16.78	16.57	17.00	16.88	17.30	16.97	15.42	16.65	16.73	16.63	17.09	17.32	16.09
CaO	0.09	0.05	0.04	0.03	0.09	0.06	0.00	0.06	0.02	0.05	0.13	0.03	0.05	0.03	0.06	0.05	0.05	0.09	0.07	0.04	0.05	0.07	0.09
Na_2O	0.00	0.02	0.03	0.02	0.03	0.02	0.01	0.00	0.06	0.03	0.02	0.00	0.00	0.01	0.04	0.00	0.01	0.00	0.00	0.00	0.04	0.04	0.01
K_2O	0.03	0.03	0.04	0.01	0.00	0.01	0.00	0.00	0.00	0.03	0.00	0.02	0.05	0.01	0.00	0.01	0.04	0.00	0.02	0.02	0.00	0.00	0.00
H_2O	11.53	11.49	11.41	11.38	11.46	11.29	11.15	11.47	11.46	11.55	11.29	11.43	11.57	11.47	11.67	11.58	11.40	11.47	11.46	11.54	11.51	11.29	11.42
Total	99.12	98.97	98.46	98.06	98.53	97.40	96.40	98.71	98.55	99.47	97.28	98.11	99.21	98.75	99.82	99.12	97.96	98.29	98.62	99.01	98.83	97.70	98.22
Si (a.p.f.u.)	5.52	5.49	5.45	5.55	5.52	5.54	5.50	5.48	5.41	5.52	5.52	5.54	5.50	5.49	5.56	5.68	5.58	5.47	5.47	5.51	5.51	5.57	5.53
Al	5.02	4.99	5.04	4.84	4.95	5.09	4.90	4.95	5.14	5.00	4.93	5.05	5.06	4.99	4.96	4.83	5.15	5.15	5.05	5.09	4.97	4.68	5.09
Fe	4.14	4.19	4.19	4.14	4.09	4.22	4.18	4.12	4.11	4.21	4.12	4.07	4.05	4.17	4.02	4.05	4.17	4.03	4.14	4.09	4.10	4.22	4.15
Mn	0.08	0.08	0.09	0.08	0.09	0.09	0.09	0.08	0.09	0.10	0.09	0.09	0.08	0.09	0.08	0.09	0.09	0.08	0.09	0.09	0.08	0.10	0.10
Mg	5.18	5.24	5.24	5.41	5.33	4.95	5.37	5.40	5.24	5.11	5.32	5.18	5.25	5.27	5.30	5.24	4.84	5.19	5.22	5.15	5.31	5.48	5.04
Ca	0.02	0.01	0.01	0.01	0.02	0.01	0.00	0.01	0.00	0.01	0.03	0.01	0.01	0.01	0.01	0.01	0.01	0.02	0.02	0.01	0.01	0.02	0.02
Na	0.00	0.01	0.01	0.01	0.01	0.01	0.00	0.00	0.02	0.01	0.01	0.00	0.00	0.00	0.02	0.00	0.00	0.00	0.00	0.00	0.02	0.02	0.00
K	0.01	0.01	0.01	0.00	0.00	0.00	0.00	0.00	0.00	0.01	0.00	0.01	0.01	0.00	0.00	0.00	0.01	0.00	0.01	0.01	0.00	0.00	0.00
Al^{IV}	2.482	2.507	2.552	2.452	2.484	2.457	2.500	2.524	2.586	2.477	2.483	2.463	2.499	2.512	2.436	2.322	2.424	2.529	2.528	2.488	2.488	2.429	2.474
Al^{VI}	2.54	2.48	2.49	2.38	2.47	2.63	2.40	2.43	2.55	2.52	2.45	2.59	2.56	2.48	2.52	2.51	2.73	2.62	2.53	2.60	2.49	2.25	2.61
Fe/(Fe Mg)	0.444	0.445	0.445	0.434	0.435	0.460	0.438	0.433	0.439	0.452	0.437	0.440	0.436	0.442	0.431	0.436	0.463	0.437	0.442	0.443	0.435	0.435	0.452
Si/Al	1.10	1.10	1.08	1.15	1.11	1.09	1.12	1.11	1.05	1.11	1.12	1.10	1.09	1.10	1.12	1.18	1.08	1.06	1.08	1.08	1.11	1.19	1.09
Ca Na K	0.03	0.03	0.03	0.02	0.03	0.03	0.00	0.01	0.03	0.03	0.04	0.01	0.02	0.01	0.03	0.01	0.03	0.02	0.02	0.01	0.03	0.03	0.02
Total cations	19.97	20.01	20.04	20.03	20.01	19.91	20.04	20.04	20.02	19.98	20.01	19.94	19.97	20.02	19.96	19.90	19.85	19.95	20.00	19.94	20.00	20.09	19.93
$\sum$ Octahedral	11.97	12.01	12.04	12.03	12.01	11.91	12.04	12.04	12.02	11.98	12.01	11.94	11.97	12.02	11.96	11.90	11.85	11.95	12.00	11.94	12.00	12.09	11.93
Cath (°C)[a]	338	342	349	333	338	334	341	344	354	337	338	335	340	342	330	312	328	345	345	339	339	329	336
K&M (°C)[a]	314	317	322	310	314	313	315	318	325	314	314	312	315	317	308	296	309	318	319	315	314	308	314
Z&F (°C)[a]	271	274	279	269	272	267	274	277	283	270	272	270	274	275	268	255	263	277	276	272	273	267	270

[a] Cath, Cathelineau (1988); K&M, Kranidiotis and MacLean (1987); Z&F, Zang and Fyfe (1995).

Table 2
Chemical composition of hydrothermal chlorites of the Cipoeiro deposit (level 185 m)

Analysis	60	62	64	66	67	68	69	70	71	72	73	74	75	76	77	79	80	81	82	83	84	85
SiO_2 (wt%)	27.38	28.59	27.96	26.55	25.19	26.83	27.83	27.40	27.77	26.52	27.35	27.41	26.08	27.28	26.54	25.99	26.34	26.73	27.80	26.30	27.51	26.71
Al_2O_3	20.04	19.44	19.54	19.11	18.97	19.57	20.52	19.44	19.64	19.87	19.71	19.36	18.28	20.50	20.82	21.06	21.49	21.15	18.99	19.24	19.13	19.98
FeO	21.17	24.43	21.11	21.56	22.31	21.47	21.59	21.49	22.13	22.11	22.43	20.56	21.44	22.11	22.66	23.37	23.92	22.67	20.99	23.48	20.60	21.33
MnO	0.33	0.34	0.18	0.33	0.37	0.34	0.31	0.31	0.38	0.34	0.33	0.37	0.33	0.29	0.36	0.36	0.40	0.34	0.32	0.35	0.35	0.36
MgO	18.47	19.56	18.44	18.78	17.67	18.04	18.12	18.74	18.27	18.43	18.60	19.51	18.09	18.19	17.54	16.91	16.62	17.75	18.55	18.17	18.48	17.98
CaO	0.08	0.07	0.07	0.03	0.06	0.08	0.07	0.13	0.07	0.09	0.07	0.00	0.02	0.05	0.01	0.05	0.00	0.03	0.08	0.06	0.41	0.02
Na_2O	0.00	0.02	0.01	0.02	0.00	0.00	0.03	0.02	0.02	0.01	0.00	0.01	0.01	0.00	0.00	0.00	0.01	0.00	0.00	0.04	0.00	0.00
K_2O	0.12	0.00	0.00	0.00	0.00	0.03	0.01	0.00	0.02	0.01	0.00	0.01	0.02	0.01	0.01	0.02	0.00	0.02	0.00	0.00	0.03	0.00
H_2O	11.64	12.12	11.64	11.42	11.08	11.44	11.77	11.61	11.69	11.53	11.68	11.62	11.11	11.71	11.59	11.51	11.63	11.70	11.54	11.46	11.51	11.46
Total	98.59	104.57	98.95	97.80	95.65	97.80	100.25	98.53	99.99	98.91	100.17	98.85	95.38	100.14	99.53	99.27	100.41	100.39	98.27	99.10	97.51	97.84
Si (a.p.f.u.)	5.642	5.656	5.763	5.579	5.455	5.627	5.672	5.662	5.699	5.519	5.615	5.657	5.630	5.587	5.492	5.417	5.431	5.479	5.777	5.506	5.732	5.593
Al	4.863	4.529	4.743	4.729	4.838	4.834	4.925	4.731	4.747	4.870	4.765	4.706	4.647	4.944	5.074	5.169	5.218	5.105	4.647	4.744	4.694	4.927
Fe	3.648	4.042	3.639	3.789	4.040	3.766	3.680	3.714	3.798	3.848	3.851	3.549	3.871	3.787	3.921	4.073	4.124	3.886	3.648	4.111	3.590	3.735
Mn	0.058	0.057	0.031	0.059	0.068	0.060	0.054	0.054	0.066	0.060	0.057	0.065	0.060	0.050	0.063	0.064	0.070	0.059	0.056	0.062	0.062	0.064
Mg	5.674	5.769	5.666	5.883	5.704	5.640	5.505	5.773	5.589	5.718	5.692	6.003	5.822	5.553	5.411	5.254	5.108	5.423	5.747	5.671	5.740	5.613
Ca	0.018	0.015	0.015	0.007	0.014	0.018	0.015	0.029	0.015	0.020	0.015	0.000	0.005	0.011	0.002	0.011	0.000	0.007	0.018	0.013	0.092	0.004
Na	0.000	0.008	0.004	0.008	0.000	0.000	0.012	0.008	0.008	0.004	0.000	0.004	0.004	0.000	0.000	0.000	0.004	0.000	0.000	0.016	0.000	0.000
K	0.032	0.000	0.000	0.000	0.000	0.008	0.003	0.000	0.005	0.003	0.000	0.003	0.006	0.003	0.003	0.005	0.000	0.005	0.000	0.000	0.008	0.000
Al_{IV}	2.358	2.344	2.237	2.421	2.545	2.373	2.328	2.338	2.301	2.481	2.385	2.343	2.370	2.413	2.508	2.583	2.569	2.521	2.223	2.494	2.268	2.407
Al_{VI}	2.51	2.19	2.51	2.31	2.29	2.46	2.60	2.39	2.45	2.39	2.38	2.36	2.28	2.53	2.57	2.59	2.65	2.58	2.42	2.25	2.43	2.52
Fe/(Fe + Mg)	0.391	0.412	0.391	0.392	0.415	0.400	0.401	0.391	0.405	0.402	0.404	0.372	0.399	0.405	0.420	0.437	0.447	0.417	0.388	0.420	0.385	0.400
Si/Al	1.16	1.25	1.22	1.18	1.13	1.16	1.15	1.20	1.20	1.13	1.18	1.20	1.21	1.13	1.08	1.05	1.04	1.07	1.24	1.16	1.22	1.14
Ca + Na + K	0.05	0.02	0.02	0.02	0.01	0.03	0.03	0.04	0.03	0.03	0.02	0.01	0.02	0.01	0.01	0.02	0.00	0.01	0.02	0.03	0.10	0.00
Total cations	19.94	20.08	19.86	20.05	20.12	19.95	19.87	19.97	19.93	20.04	20.00	19.99	20.05	19.94	19.97	19.99	19.96	19.96	19.89	20.12	19.92	19.94
∑ Octahedral	11.94	12.08	11.86	12.05	12.12	11.95	11.87	11.97	11.93	12.04	12.00	11.99	12.05	11.94	11.97	11.99	11.96	11.96	11.89	12.12	11.92	11.94
Cath (°C)[a]	318	315	298	328	348	320	313	314	309	337	322	315	320	327	342	354	352	344	296	340	303	326
K&M (°C)[a]	297	297	284	304	319	299	294	295	292	311	301	294	299	304	315	324	323	316	282	314	287	303
Z&F (°C)[a]	263	260	250	270	281	264	259	261	256	275	265	263	264	268	276	283	280	278	249	275	254	268

[a] Cath, Cathelineau (1988); K&M, Kranidiotis and MacLean (1987); Z&F, Zang and Fyfe (1995).

Table 3
Chemical composition of hydrothermal chlorites of the Cipoeiro deposit (level 201 m)

Analysis	86	87	88	90	92	93	94	95	96	97	98	99	101	102	103	104	105	106	109	110	111	112	113	114	115
SiO_2 (wt%)	25.56	26.41	24.35	26.73	27.14	27.93	27.42	27.92	26.87	27.34	26.88	27.04	27.91	27.17	27.78	26.85	26.79	26.72	27.62	26.51	26.27	26.86	27.17	27.25	26.87
Al_2O_3	21.21	19.08	18.62	21.56	20.38	19.81	21.01	19.70	20.78	19.87	20.39	20.84	21.62	20.50	19.41	20.80	20.15	20.71	20.20	20.08	18.91	20.47	20.18	20.03	20.83
FeO	24.27	22.30	22.68	22.86	22.46	21.13	22.90	21.00	23.01	22.17	21.42	23.22	23.02	21.88	20.97	22.97	22.71	22.36	21.81	23.14	22.65	22.71	21.89	22.07	21.95
MnO	0.40	0.37	0.38	0.40	0.38	0.35	0.40	0.24	0.38	0.37	0.43	0.39	0.39	0.40	0.36	0.45	0.41	0.35	0.41	0.35	0.37	0.35	0.38	0.33	0.36
MgO	15.32	18.23	16.69	16.12	18.33	18.70	17.31	19.14	17.27	18.02	18.43	17.31	15.96	17.97	19.16	16.84	17.09	17.75	18.32	16.80	17.66	16.84	17.28	17.86	17.34
CaO	0.02	0.04	0.05	0.05	0.01	0.03	0.02	0.03	0.00	0.04	0.01	0.06	0.11	0.03	0.03	0.05	0.03	0.04	0.06	0.05	0.06	0.00	0.01	0.06	0.04
Na_2O	0.03	0.00	0.00	0.00	0.00	0.00	0.00	0.03	0.01	0.00	0.00	0.00	0.02	0.01	0.00	0.01	0.00	0.01	0.00	0.00	0.00	0.00	0.02	0.01	0.00
K_2O	0.03	0.00	0.02	0.00	0.03	0.00	0.05	0.02	0.00	0.00	0.04	0.00	0.08	0.00	0.00	0.03	0.01	0.01	0.00	0.01	0.00	0.00	0.01	0.01	0.02
H_2O	11.32	11.37	10.78	11.58	11.72	11.72	11.77	11.74	11.63	11.61	11.62	11.70	11.79	11.66	11.68	11.59	11.49	11.61	11.73	11.42	11.28	11.51	11.52	11.60	11.58
Total	98.16	97.80	93.57	99.30	100.45	99.67	100.88	99.82	99.95	99.42	99.22	100.56	100.1	99.62	99.39	99.59	98.68	99.56	100.15	98.36	97.20	98.74	98.46	99.22	98.99
Si (a.p.f.u.)	5.415	5.571	5.417	5.539	5.556	5.718	5.590	5.704	5.540	5.646	5.550	5.545	5.679	5.591	5.706	5.558	5.595	5.518	5.648	5.569	5.588	5.600	5.658	5.637	5.567
Al	5.292	4.740	4.878	5.261	4.913	4.776	5.044	4.740	5.046	4.833	4.958	5.033	5.181	4.968	4.695	5.071	4.956	5.037	4.865	4.968	4.737	5.026	4.949	4.879	5.083
Fe	4.300	3.934	4.220	3.961	3.845	3.618	3.904	3.588	3.968	3.829	3.699	3.982	3.917	3.766	3.602	3.977	3.967	3.862	3.730	4.066	4.029	3.959	3.812	3.818	3.803
Mn	0.072	0.066	0.072	0.070	0.066	0.061	0.069	0.042	0.066	0.065	0.075	0.068	0.067	0.070	0.063	0.079	0.073	0.061	0.071	0.062	0.067	0.062	0.067	0.058	0.063
Mg	4.838	5.733	5.535	4.980	5.594	5.707	5.261	5.830	5.308	5.548	5.673	5.291	4.841	5.513	5.867	5.197	5.321	5.465	5.585	5.262	5.600	5.234	5.365	5.508	5.356
Ca	0.005	0.009	0.012	0.011	0.002	0.007	0.004	0.007	0.000	0.009	0.002	0.013	0.024	0.007	0.007	0.011	0.007	0.009	0.013	0.011	0.014	0.000	0.002	0.013	0.009
Na	0.012	0.000	0.000	0.000	0.000	0.000	0.000	0.012	0.004	0.000	0.000	0.000	0.008	0.004	0.000	0.004	0.000	0.004	0.000	0.000	0.000	0.000	0.008	0.004	0.000
K	0.008	0.000	0.006	0.000	0.008	0.000	0.013	0.005	0.000	0.000	0.011	0.000	0.021	0.000	0.000	0.008	0.003	0.003	0.000	0.003	0.000	0.000	0.003	0.003	0.005
Al^{IV}	2.585	2.429	2.583	2.461	2.444	2.282	2.410	2.296	2.460	2.354	2.450	2.455	2.321	2.409	2.294	2.442	2.405	2.482	2.352	2.431	2.412	2.400	2.342	2.363	2.433
Al^{VI}	2.71	2.31	2.30	2.80	2.47	2.49	2.63	2.44	2.59	2.48	2.51	2.58	2.86	2.56	2.40	2.63	2.55	2.56	2.51	2.54	2.33	2.63	2.61	2.52	2.65
Fe/(Fe + Mg)	0.471	0.407	0.433	0.443	0.407	0.388	0.426	0.381	0.428	0.408	0.395	0.429	0.447	0.406	0.380	0.434	0.427	0.414	0.400	0.436	0.418	0.431	0.415	0.409	0.415
Si/Al	1.02	1.18	1.11	1.05	1.13	1.20	1.11	1.20	1.10	1.17	1.12	1.10	1.10	1.13	1.22	1.10	1.13	1.10	1.16	1.12	1.18	1.11	1.14	1.16	1.10
Ca + Na + K	0.03	0.01	0.02	0.01	0.01	0.01	0.02	0.02	0.00	0.01	0.01	0.01	0.05	0.01	0.01	0.02	0.01	0.02	0.01	0.01	0.01	0.00	0.01	0.02	0.01
Total cations	19.94	20.05	20.14	19.82	19.98	19.89	19.89	19.93	19.93	19.93	19.97	19.93	19.74	19.92	19.94	19.91	19.92	19.96	19.91	19.94	20.04	19.88	19.86	19.92	19.89
∑ Octahedral	11.94	12.05	12.14	11.82	11.98	11.89	11.89	11.93	11.93	11.93	11.97	11.93	11.74	11.92	11.94	11.91	11.92	11.96	11.91	11.94	12.04	11.88	11.86	11.92	11.89
Cath (°C)[a]	354	329	354	334	332	305	326	308	334	317	333	333	312	326	307	331	325	338	317	329	326	324	315	318	330
K&M (°C)[a]	327	306	324	312	307	289	305	290	311	298	307	310	297	303	289	309	305	312	297	308	305	304	297	299	307
Z&F (°C)[a]	280	269	283	269	271	255	265	258	271	261	273	270	254	267	257	268	265	274	262	267	266	264	259	262	269

[a] Cath, Cathelineau (1988); K&M, Kranidiotis and MacLean (1987); Z&F, Zang and Fyfe (1995).

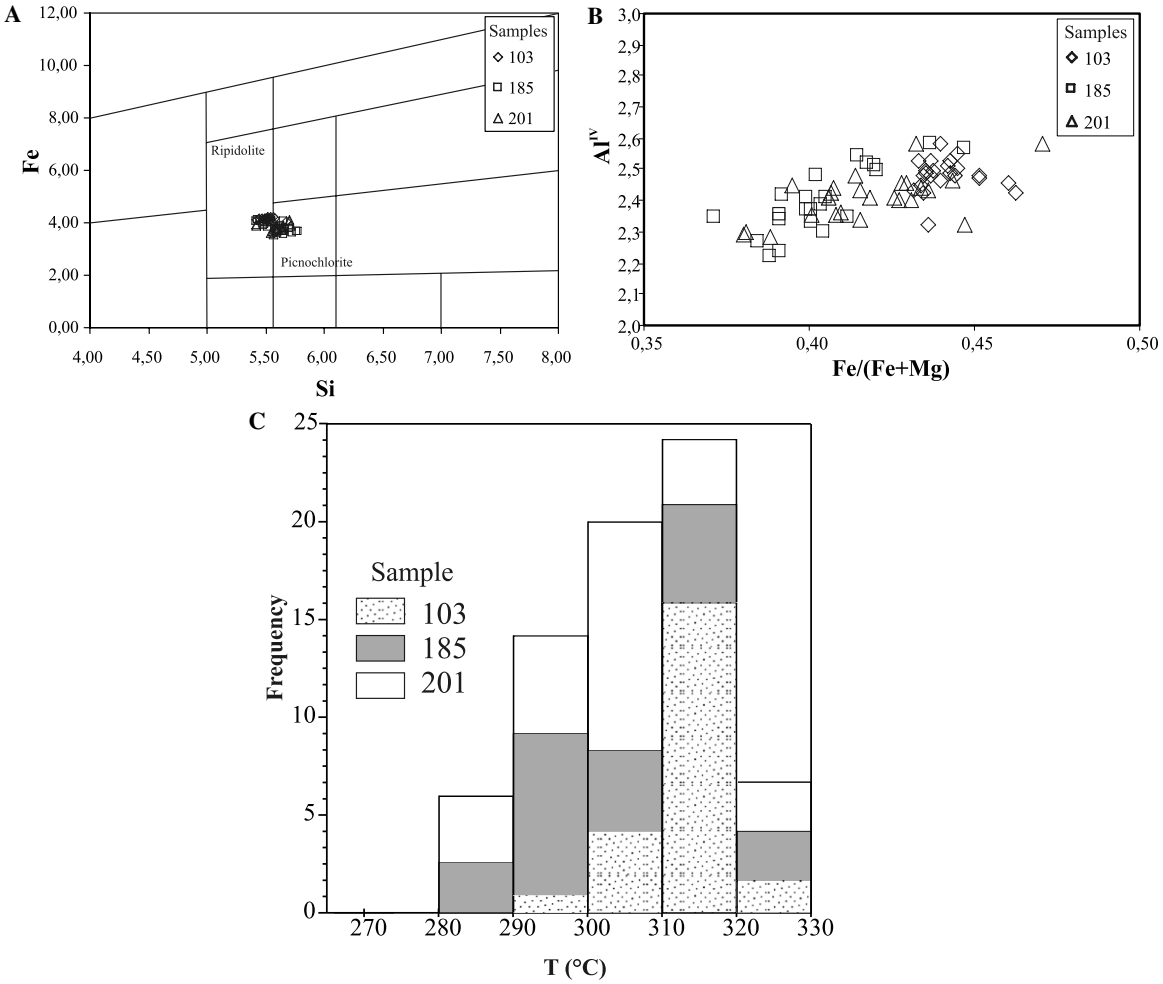

Fig. 5. (A) Classification of the hydrothermal chlorites of the Cipoeiro deposit based on Hey (1954). (B) Diagram showing covariance between the Fe/(Fe + Mg) ratio and Al^{IV}. (C) Frequency histograms of the calculated temperatures of chlorite formation based on the geothermometer of Kranidiotis and MacLean (1987).

6. Stable isotope geochemistry

6.1. Isotope results

Isotope results appear in Table 5. Three samples of calcite were analyzed for carbon and oxygen isotopes. The $\delta^{13}C$ value is −4.3‰ in the matrix of the microtonalite and −6.1‰ and −6.3‰ in the veinlets of the intermediate and lower mineralized zones in the tonalite. The $\delta^{18}O$ value of calcite is +9.5‰ in the microtonalite and +9.9‰ in the tonalite. The quartz samples show $\delta^{18}O$ values of +7.8‰ in the microtonalite, +9.1‰ and +9.6‰ in quartz-carbonate veinlets from different alteration zones of the hosting tonalites, and +11.9‰ in a thick mineralized quartz vein. White mica shows $\delta^{18}O$ values of +4.9‰ and +8.6‰ in two mineralized zones hosted in the tonalite. The δD values of these white mica samples are −18‰ and −42‰, respectively. Two chlorite samples have $\delta^{18}O$ values of +5.9‰ and +7.3‰ and δD of −26‰ and −71‰, respectively, in the microtonalite and the lower zone of the tonalite. The water extracted from fluid inclusions from the thick quartz vein displays a δD value of −30‰, whereas the $\delta^{13}C$ value of the extracted CO_2 is −10.7‰. The $\delta^{34}S$ values of two tonalite-hosted ore-related pyrite samples are +1.1‰ and +1.7‰.

6.2. Oxygen isotope geothermometry

The quartz–muscovite and quartz–chlorite (Zheng, 1993) oxygen isotope geothermometers were employed but not the quartz–calcite geothermometer because of the clear oxygen isotope disequilibrium ($\delta^{18}O$ quartz $< \delta^{18}O$ calcite; see subsequent discussion). The results appear in Table 6. Most of the calculated temperatures are too high (>800 °C) and not geologically significant, considering the mineral paragenesis, structural setting, and chlorite thermometry. This finding may indicate a lack of isotopic equilibrium, which can arise from precipitation of the mineral pairs at distinct stages of the paragenetic sequence or isotope exchange during retrogression. Only the quartz–muscovite pair of the 185 m level furnished a realistic value of 319 °C, which is in good agreement with the temperature values obtained from the chlorite geothermometry (Table 6).

Table 4
Chemical composition of hydrothermal white micas of the Cipoeiro deposit

Sample:	PD179/103		PD179/201		
Analysis no.:	53	57	91	100	108
SiO_2 (wt%)	48.97	48.78	49.22	45.00	48.78
Al_2O_3	28.30	28.35	28.10	27.49	28.16
MgO	2.30	3.01	2.98	5.09	3.29
FeO	3.42	3.80	2.71	6.37	3.02
MnO	0.03	0.00	0.01	0.11	0.02
CaO	0.05	0.03	0.04	0.00	0.09
Na_2O	0.07	0.09	0.09	0.08	0.09
K_2O	11.57	11.17	11.47	9.41	10.99
H_2O	4.00	4.00	4.00	4.00	4.00
Total	98.70	99.22	98.61	97.54	98.44
Si	6.71	6.65	6.72	6.31	6.67
Al^{IV}	1.28	1.34	1.27	1.68	1.32
Al^{VI}	5.42	5.31	5.45	4.63	5.36
Fe^{+2}	0.39	0.43	0.30	0.74	0.34
Mg	0.47	0.61	0.60	1.06	0.67
Mn	0.00	0.00	0.00	0.01	0.00
Ca	0.00	0.00	0.00	0.00	0.01
Na	0.02	0.02	0.02	0.02	0.02
K	2.02	1.94	2.00	1.68	1.92
OH	3.65	3.64	3.64	3.74	3.65
Total	17.85	17.86	17.84	18.13	17.84

6.3. Fluid composition and potential sources

The isotopic composition of the fluid was calculated from the mineral analyses, assuming local equilibrium between the minerals and the precipitating fluid and using the appropriate mineral–water fractionation factors. The temperature range of 305–319 °C was chosen to estimate the fluid composition, with the extreme values corresponding to the modal value obtained from chlorite thermometry and the temperature obtained from the oxygen isotope thermometry, respectively. The calculated isotopic compositions appear in Table 7.

Considering that quartz is much more resistant than carbonates, micas, and chlorite to oxygen isotope changes after mineral precipitation (Gregory and Criss, 1986), only the oxygen isotope compositions calculated from quartz analyses are used here. The oxygen isotope composition of the fluid was calculated from the quartz–water (Matsuhisa et al., 1979) pair. The $\delta^{18}O$ values of the fluid calculated from quartz are +1.1‰ to +1.6‰ in the microtonalite, +2.4‰ to +3.4‰ in quartz-carbonate veinlets cutting the tonalite, and +5.2‰ to +5.7‰ in the thick quartz vein (Table 7). These distinct values in different host rocks and/or structural styles probably record precipitation of quartz in distinct alteration stages (Fig. 4) from hydrothermal fluids with distinct compositions or slightly different temperatures. Furthermore, the values found in quartz from the microtonalite may reflect the magmatic oxygen composition of the quartz.

Fluid δD values were measured directly in inclusion fluids and calculated from the hydrous mineral analysis. The δD value of the fluid obtained from the chlorite–water fractionation factor of Graham et al. (1987) are +2‰ and −43‰ in samples 103 and 201, respectively. The first value is probably too high for this type of deposit, which in general shows δD values lower than −10‰ (see McCuaig and Kerrich, 1998), unless evaporite or sedimentary brines are present (Ohmoto, 1986; Kerrich, 1987), which is unlikely

Table 5
Isotopic data from alteration-related minerals of the Cipoeiro gold deposit

Sample	Host rock	Mineral	Sampling site	Silicates		Carbonates		Fluid inclusions		Sulfides
				$\delta^{18}O$ (‰)	δD (‰)	$\delta^{13}C$ (‰)	$\delta^{18}O$ (‰)	$\delta^{13}C_{CO_2}$ (‰)	δD_{H_2O} (‰)	$\delta^{34}S$ (‰)
PD179/103	Microtonalite	Quartz	Alter zone	+7.8						
PD179/103	Microtonalite	Chlorite	Alter zone	+5.9	−26					
PD179/103	Microtonalite	Calcite	Alter zone			−4.3	+9.5			
PD179/185	Tonalite	Quartz	Veinlet	+9.6						
PD179/185	Tonalite	Calcite	Veinlet			−6.1	+9.9			
PD179/185	Tonalite	White mica	Alter zone	+4.9	−18					
PD179/185	Tonalite	Pyrite	Alter zone							+1.7
PD179/201	Tonalite	Quartz	Veinlet	+9.1						
PD179/201	Tonalite	Calcite	Veinlet			−6.3	+9.9			
PD179/201	Tonalite	White mica	Alter zone	+8.6	−42					
PD179/201	Tonalite	Chlorite	Alter zone	+7.3	−71					
PD179/201	Tonalite	Pyrite	Alter zone							+1.1
PD179/216	Tonalite	Quartz	Vein	+11.9				−10.7	−30	

Table 6
Temperatures obtained by oxygen isotope thermometry in samples of the Cipoeiro deposit compared with those obtained by the chlorite geothermometer

Sample/level	$\delta^{18}O$qz measured (‰)	$\delta^{18}O$mus measured (‰)	T (°C) Zheng (1993)	$\delta^{18}O$chl measured (‰)	T (°C) Zheng (1993)	T (°C) chlorite
PD179/103	7.8	–	–	5.9	889	315
PD179/185	9.6	4.9	319	–	–	302
PD179/201	9.1	8.6	1542	7.3	921	305

Notes: qz, quartz; mus, white mica; chl, chlorite. Chlorite temperatures are average values for each sample.

Table 7
Calculated (and measured) isotope compositions of the fluid in equilibrium with minerals in the Cipoeiro deposit for temperature range 305–319 °C (see text for discussion and fractionation factors)

Sample	Mineral	$\delta^{18}O_{H_2O}$(‰)	δD_{H_2O} (‰)	$\delta^{13}C_{CO_2}$(‰)	$\delta^{34}S_{H_2S}$(‰)
PD179/103	Quartz	+1.1 to +1.6			
PD179/103	Chlorite	+5.9 to +6.1	+2		
PD179/103	Calcite	+4.1 to +4.5		−2.2 to −2.1	
PD179/185	Quartz	+2.9 to +3.4[a]			
PD179/185	Calcite	+4.4 to +4.8		−4.0 to −3.9	
PD179/185	White mica	+1.7 to +2.0	−20[a]		
PD179/185	Pyrite				+0.5 to +0.6
PD179/201	Quartz	+2.4 to +2.9[a]			
PD179/201	Calcite	+4.5 to +4.9		−4.2 to −4.1	
PD179/201	White mica	+5.4 to +5.7	−21[a]		
PD179/201	Chlorite	+7.3 to +7.5	−43[a]		
PD179/201	Pyrite				−0.1 to 0.0
PD179/216	Quartz	+5.2 to +5.7[a]	−30[a]	−10.7	

[a] Values used as estimations of the oxygen–hydrogen isotopes composition of the mineralizing fluid (see Fig. 6).

in the studied region. This positive value likely reflects isotopic disequilibrium or exchange at lower temperatures (e.g., Kerrich, 1987). The second value is more consistent with the δD value of −30‰ measured on waters extracted from fluid inclusions. For the white mica–water pair, the fractionation factor of Suzuoki and Epstein (1976) was employed, with the correction proposed by Lambert and Epstein (1980), yielding δD values of −20‰ and −21‰ in two samples, in reasonable agreement with the value obtained directly from fluid inclusion analysis.

As a whole, the δ^{18}O values of the fluid estimated from quartz are lower than those of the magmatic range, as defined by Sheppard (1986). A contribution from the hosting tonalite is discarded, on the basis of the age difference between the host rock and the mineralization (>50 Ma). Syntectonic (peraluminous, collision-type) granitoids could have contributed fluids, but combined fluid δ^{18}O and δD values indicate metamorphic fluids as the more probable, or at least predominant, sources for the oxygen and hydrogen of the fluids at Cipoeiro (Fig. 6).

The δ^{13}C value of the fluid CO_2 was obtained directly by measuring the δ^{13}C of the CO_2 extracted from fluid inclusions and the calcite–CO_2 fractionation factor of Ohmoto and Rye (1979). The δ^{13}C value of fluid inclusion CO_2 obtained in a single sample is −10.7‰, whereas the values calculated for the CO_2 in equilibrium with calcite are −2.1‰ to −2.2‰ in the ore zone hosted in the microtonalite, and −3.9‰ to −4.2‰ in the zones hosted in the tonalite. The relatively large difference (~6‰) between the carbon isotope composition of fluid inclusion CO_2 and carbonate CO_2 may indicate that the carbonates precipitated from a fluid with a distinct composition from the fluid trapped in the fluid inclusions. This proposition is in keeping with structural, petrographic, and oxygen isotope evidence, which indicates that the formation of quartz veins and the hydrothermal alteration of the hosting tonalites occurred in distinct stages or at slightly distinct temperatures. Nevertheless, the overall values are in the range considered normal for this type of deposit (e.g., McCuaig and Kerrich, 1998) and are not diagnostic of a unique source, because they overlap the fields of mantle, magmatic, and metamorphic carbon reservoirs (Ohmoto, 1986; McCuaig and Kerrich, 1998). They might also reflect mixing sources.

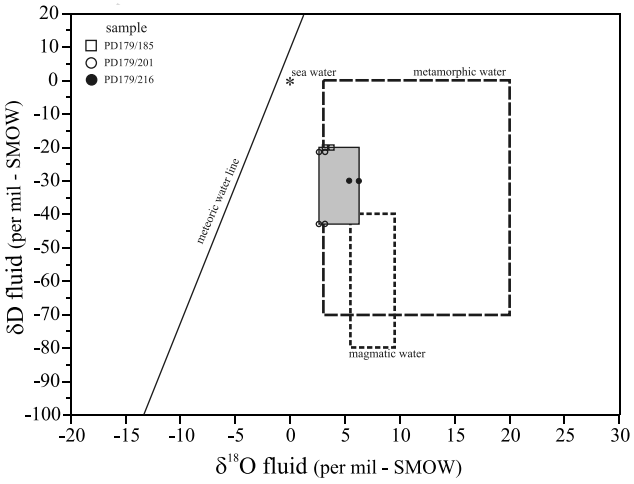

Fig. 6. Diagram showing the estimated isotope composition of the mineralizing fluid (shaded area) at Cipoeiro. The δ^{18}O value of the fluid was calculated from quartz analyses, and δD was calculated from muscovite and chlorite analyses or measured in fluid inclusions (see also Table 7 and discussions in the text). The magmatic and metamorphic fields are from Sheppard (1986).

The δ^{34}S value of the fluid was estimated from the pyrite-H_2S fractionation factor of Ohmoto and Rye (1979), assuming H_2S as the main sulfur species in the fluid. The fluid δ^{34}S values range from −0.1‰ to +0.5‰, interpreted as reflecting a magmatic or mantle source, or alternatively, an average crustal sulfur composition (Ohmoto and Rye, 1979; Lambert et al., 1984). These values indicate that the redox state of the fluid was below the SO_2/H_2S buffer (Kerrich, 1989), that is, that it was relatively reduced.

7. Summary and concluding remarks

The Cipoeiro gold deposit, located in the Gurupi Belt, is hosted by tonalites of 2148 Ma belonging to a major suite

of calc-alkaline orogenic granitoids. At a regional scale, the deposit is related to the strike-slip Tentugal shear zone, close to the boundary zone between the Gurupi Belt and the São Luís Craton. At the deposit scale, the ore bodies are controlled by splays geometrically related to this major shear zone, with mineralized zones confined to discrete ductile–brittle shear zones that cut across the tonalites, close to the contact with a metasedimentary unit.

The styles of mineralization are comprised of thick quartz veins and disseminations in discrete shear zones associated with narrow and discontinuous quartz-carbonate veinlets, always accompanied by sulfidation of the host rock. The hydrothermal paragenesis is postmetamorphic and composed of quartz, calcite, chlorite, phengite, pyrite, and minor albite.

The chemical composition of the hydrothermal chlorites, especially the Fe/(Fe + Mg) ratios and Al^{IV} contents, are relatively uniform over depths of 100 m and yield a relatively narrow interval of 305 ± 15 °C for the equilibrium of the chlorites with the hydrothermal fluid.

Stable isotope (O, H, C, S) compositions have been determined in silicate, carbonate, and sulfide minerals, as well as in inclusion fluids. The measured and calculated $\delta^{18}O$ and δD values of the mineralizing fluid range from +2.4 to +5.7 and from −43 to −20, respectively. These values are more consistent with a metamorphic origin, in keeping with the interpretation of postmetamorphic timing for the mineralizing episode. As such, devolatilization reactions that occurred during metamorphism of the nearby metavolcanosedimentary sequence likely produced the ore-bearing fluids. The $\delta^{13}C$ values of fluid CO_2 are in the range −10.7 to −3.9, whereas the fluid $\delta^{34}S$ is around 0‰. Carbon and sulfur compositions are not diagnostic of their sources, because they are compatible with mantle, magmatic, or average crustal reservoirs. They likely reflect some leaching of carbon and sulfur of the rocks through which they passed during fluid migration.

Combined chlorite and oxygen isotope thermometry defines a narrow temperature range of 305–319 °C for the precipitation of the ore. The hydrothermal paragenesis, chlorite–pyrite coexistence, temperature of ore formation, and sulfur isotope evidence indicate relatively low (reduced) fO_2 conditions for the mineralizing fluid. Collectively, the tectonic setting and geologic, chemical, and isotopic characteristics of the Cipoeiro deposit are similar to those described elsewhere for deposits hosted in plutono-metamorphic belts of all ages and classified as orogenic gold deposits (e.g., Groves et al., 1998).

Acknowledgments

Financial support for this study came from CAPES (BEX 2020/02-05), CPRM/Geological Survey of Brazil, and UFPA. The paper is a contribution to the project PRONEX/CNPq/UFPA (66.2103/1998). The authors are thankful to the staff of Santa Fé do Brasil (C. Torresini, G.M. Brandão, J.W. Ribeiro, S.J.C. Melo) for field support and discussions on the geology of the deposit; J.L. Devidal (Université Blaise Pascal, Clermont Ferrand) for helping during the microprobe work; and C. Renac (Université Jean Monnet, Saint Etienne) for technical support and discussions during E.L.K.'s sabbatical leave at Saint Etienne. Constructive comments and suggestions of Dave Craw and an anonymous reviewer helped improve the manuscript, and they are acknowledged.

References

Bailey, S.W., 1980. Summary of recommendations of AIPEA nomenclature committee on clay minerals. American Mineralogist 65, 1–7.

Bayliss, P., 1975. Nomenclature of the trioctahedral chlorites. Canadian Mineralogist 13, 178–180.

Cathelineau, M., 1988. Cation site occupancy in chlorites and illites as a function of temperature. Clay Minerals 23, 471–485.

Clayton, R.N., Mayeda, T.K., 1963. The use of bromine pentafluoride in the extraction of oxygen from oxides and silicates from isotopic analyses. Geochimica et Cosmochimica Acta 27, 43–52.

Coleman, M.L., Shepherd, T.J., Durham, J.J., Rouse, J.E., Moore, G.R., 1982. Reduction of water with zinc for hydrogen isotope analysis. Analytical Chemistry 54, 993–995.

Costa, J.B.S., Pastana, J.M.N., Costa, E.J.S., Jorge-João, X.S., 1988. A faixa de cisalhamento Tentugal na Folha SA.23-Y-B. 35 Congresso Brasileiro de Geologia, Belém, v. 5, pp. 2257–2266.

Costa, J.L., Almeida, H.G.G., Ricci, P.S.F., 1996. Metamorfismo e divisão tectono-estratigráfica do Grupo Gurupi no nordeste do Pará e noroeste do Maranhão: 5 Simpósio de Geologia da Amazônia, Belém, pp. 110–112.

De Caritat, P., Hutcheon, I., Walshe, J.L., 1993. Chlorite geothermometry: a review. Clays and Clay Minerals 41, 219–239.

Graham, C.M., Viglino, J.A., Harmon, R.S., 1987. Experimental study of hydrogen-isotope exchange between aluminous chlorite and water and of hydrogen diffusion in chlorite. American Mineralogist 72, 566–579.

Gregory, R.T., Criss, R.E., 1986. Isotopic exchange in open and closed systems. In: Valley, J.W., Taylor, H.P., Jr., O'Neil, J.R. (Eds.), Stable Isotopes in High Temperature Geological Processes, Mineral. Soc. America, Reviews in Mineralogy, vol. 16, pp. 91–127.

Groves, D.I., Goldfarb, R.J., Gebre-Mariam, M., Hagemann, S.G., Robert, F., 1998. Orogenic gold deposits: a proposed classification in the context of their crustal distribution and relationship to other gold deposit types. Ore Geology Reviews 13, 7–27.

Harris, C., Stuart Smith, H., le Roex, A.P., 2000. Oxygen isotope composition of phenocrysts from Tristan da Cunha and Gough island lavas: variation with fractional crystallization and evidence for assimilation. Contributions to Mineralogy and Petrology 138, 164–175.

Hey, M.H., 1954. A new review of the chlorites. Mineralogical Magazine 30, 277–292.

Jiang, W.T., Peacor, D.R., Buseck, P.R., 1994. Chlorite geothermometry? – contamination and apparent octahedral vacancies. Clays and Clay Minerals 42, 593–605.

Kerrich, R., 1987. The stable isotope geochemistry of Au–Ag vein deposits in metamorphic rocks. In: Kyser, T.K. (Ed.), Stable Isotope Geochemistry of Low Temperature Fluids. Mineralogical Association of Canada, Short Course, Germany, pp. 287–336.

Kerrich, R., 1989. Geochemical evidence on the sources of fluids and solutes for shear zone hosted mesothermal Au deposits. In: Bursnall, J.T. (Ed.), Mineralization and Shear Zones. Geological Association of Canada Short Course Notes, vol. 6, pp. 129–197.

Klein, E.L., Moura, C.A.V., 2001. Age constraints on granitoids and metavolcanic rocks of the São Luís craton and Gurupi belt, northern Brazil: implications for lithostratigraphy and geological evolution. International Geology Review 43, 237–253.

Klein, E.L., Moura, C.A.V., 2003. Síntese geológica e geocronológica do Cráton São Luís e do Cinturão Gurupi na região do rio Gurupi (NE-Para/NW-Maranhão). Revista Geologia USP, Série Científica 3, 97–112.

Klein, E.L., Moura, C.A.V., Krymsky, R., Griffin, W.L., 2005. The Gurupi belt in northern Brazil: lithostratigraphy, geochronology, and geodynamic evolution. Precambrian Research 141, 83–105.

Kranidiotis, P., MacLean, W.H., 1987. Systematics of chlorite alteration at the Phelps Dodge massive sulfide deposit, Matagami, Quebec. Economic Geology 82, 1898–1911.

Lambert, S.J., Epstein, S., 1980. Stable isotope investigations of an active geothermal system in Valles Caldera, Jemez Mountains, New Mexico. Journal of Volcanology and Geothermal Research 8, 111–129.

Lambert, I.B., Phillips, G.N., Groves, D.I., 1984. Sulfur isotope compositions and genesis of Archaean gold mineralization, Australia and Zimbabwe. In: Foster, R.P., (Ed.), Geological Society of Zimbabwe Special Publication, vol. 1, pp. 373–387.

Matsuhisa, Y., Goldschmit, J.R., Clayton, R.N., 1979. Oxygen isotope fractionation in the system quartz–albite–anorthite–water. Geochimica et Cosmochimica Acta 43, 1131–1140.

McCuaig, T.C., Kerrich, R., 1998. P–T–t-deformation-fluid characteristics of lode gold deposits: evidence from alteration systematics. Ore Geology Reviews 12, 381–453.

McRae, M., 1950. The isotopic chemistry of carbonates and a paleotemperature scale. Journal of Chemical Physics 18, 849–857.

Ohmoto, H., 1986. Stable isotope geochemistry of ore deposits. In: Valley, J.W., Taylor Jr., H.P., O'Neil, J.R. (Eds.), Stable Isotopes in High Temperature Geological Processes. Mineralogical Society of America, Reviews in Mineralogy, vol. 16, pp. 491–559.

Ohmoto, H., Rye, R.O., 1979. Isotopes of sulfur and carbon. In: Barnes, H.L. (Ed.), Geochemistry of Hydrothermal Ore Deposits. John Wiley & Sons, pp. 509–567.

Palheta, E.S.M., 2001. Evolução geológica da região nordeste do Estado do Pará com base em estudos estruturais e isotópicos de granitóides. Unpub. MSc Thesis, Universidade Federal do Pará, Belém, Brazil, 144 p.

Pastana, J.M.N., 1995. Programa Levantamentos Geológicos Básicos do Brasil. Programa Grande Carajás. Turiaçu/Pinheiro, folhas SA.23-V-D/SA.23-Y-B. Estados do Pará e Maranhão. CPRM, 205 p.

Pinheiro, B.L.S., Moura, C.A.V., Klein, E.L., 2003. Estudo de proveniência em arenitos das formações Igarapé de Areia e Viseu, nordeste do Para, com base em datação de monocristais de zircão por evaporação de chumbo. 8 Simpósio de Geologia da Amazônia, Manaus. Resumos expandidos (CD-ROM).

Ribeiro, J.W.A., 2002. O arcabouço estrutural da região de Chega Tudo e Cedral, NW do Maranhão, com base em sensores geofisicos. Unpub. MSc thesis. Universidade Federal do Pará, Belém, Brazil, 155 p.

Schiffman, P., Fridleifsson, G.O., 1991. The smectite–chlorite transition in drillhole NJ-15, Nesjavellir geothermal field, Iceland: XRD, BSE and electron microprobe investigations. Journal of Metamorphic Geology 9, 679–696.

Sheppard, S.M.F., 1986. Characterization and isotopic variations in natural waters. In: Valley J.W., Taylor H.P., O'Neil J.R. (Eds.), Stable Isotopes in High Temperature Geological Processes. Mineralogical Society of America, Reviews in Mineralogy, vol. 16, pp. 165–183.

Suzuoki, T., Epstein, S., 1976. Hydrogen isotope fractionation between OH-bearing minerals and water. Geochimica et Cosmochimica Acta 40, 1229–1240.

Torresini, C., 2000. The Gurupi gold deposits (Cipoeiro and Chega Tudo), Gurupi Belt, Pará, Brazil; geology and mineralization. 4 International Gold Symposium, Lima, Peru (on CD-ROM).

Vennemann, T.W., O'Neil, J.R., 1993. A simple and inexpensive method for hydrogen isotope and water analyses of minerals and rocks based on zinc reagent. Chemical Geology Isotope Geosciences Section 103, 227–234.

Vidal, O., Parra, T., Trotet, F., 2001. A thermodynamic model for Fe–Mg aluminous chlorite using data from phase equilibrium experiments and natural pelitic assemblages in the 100° to 600 °C and 1 to 25 kb range. American Journal of Science 301, 557–592.

Yamaguti, H.S., Villas, R.N.N., 2003. Estudo microtermométrico dos fluidos hidrotermais relacionados com a mineralização aurífera de Montes Áureos, NW do Maranhão. Revista Brasileira de Geociências 33, 21–32.

Zang, W., Fyfe, W.S., 1995. Chloritization of the hydrothermally altered bedrock at the Igarapé Bahia gold deposit, Carajás, Brazil. Mineralium Deposita 30, 30–38.

Zheng, Y.F., 1993. Calculation of oxygen isotope fractionation in hydroxyl-bearing silicates. Earth and Planetary Sciences Letters 120, 247–263.